

DEVELOPMENTAL BIOLOGY

Acquisition of neural crest promoted thyroid evolution from chordate endostyle

Jan Stundl^{1,2*}, Ayyappa Raja Desingu Rajan^{1†}, Hugo A. Urrutia^{1†}, Jake Leyhr^{3‡}, Jana Stundlova¹, Tatiana Solovieva¹, Tatjana Haitina³, Sophie Sanchez³, Zuzana Musilova⁴, Megan L. Martik^{1§}, Marianne E. Bronner^{1*}

The endostyle is an endodermal organ unique to nonvertebrate chordates except for lamprey larvae, where it serves as forerunner to the adult thyroid. Here, we examine whether the acquisition of neural crest in the vertebrate lineage played a role in the elaboration of the endostyle. CM-Dil lineage tracing reveals a neural crest contribution to the endostyle, and CRISPR-Cas9 mutagenesis of key neural crest genes causes endostyle defects including formation of a single rather than bilobed structure. RNA sequencing reveals gene profiles characteristic of embryonic neural crest cells and Schwann cell precursors in the developing endostyle. Contrasting with the prevailing view that the endostyle is an endoderm-derived organ, we propose that the acquisition of the neural crest played a critical step in promoting thyroid evolution from chordate endostyle.

INTRODUCTION

In the deuterostome lineage, the chordate body plan is unique with notable features including a dorsal nerve cord, notochord, and complex pharyngeal region. Rather than simply representing the anterior part of the alimentary system, the chordate pharynx is a remarkable developmental innovation that gives rise to various organs and structures that serve a wide range of functions, including prey capture and respiration (1). In addition to structures associated with feeding and breathing, the pharyngeal wall forms specialized endocrine glands like the thyroid and parathyroid glands, thymus, and ultimobranchial bodies (2, 3).

The thyroid gland is an evolutionary novelty of vertebrates and is the first endocrine organ to develop during vertebrate embryogenesis, appearing approximately 3 to 5 weeks after gestation in humans (4). It develops from a thickening in the midventral part of the pharyngeal floor, descending along the thyroglossal duct to its final position in the neck. In mammals, the developing thyroid fuses with the parathyroid glands and ultimobranchial bodies (5, 6), forming a complex organ here referred to as the “thyroid complex” (Fig. 1A). In contrast to mammals, the glands of the thyroid complex in birds and amphibians are separate and located in the cervicothoracic region (Fig. 1, B and C) (5, 7). In ray-finned fishes, the thyroid appears as dispersed follicles in the branchial region and does not form a compacted gland (5, 8).

While the thyroid gland primarily develops from the endoderm (9), classical quail-chick grafting experiments have revealed an additional contribution from the neural crest (NC) (10–12). Similarly,

fate-mapping studies in mice have suggested a NC contribution (13, 14). To validate a NC contribution to the individual components of the thyroid complex using current techniques, we performed intraspecific homotopic grafts of dorsal neural tubes from green fluorescent protein (GFP) transgenic chick embryos into the neck region of unlabeled chick hosts (Fig. 1, D to F). Our results confirm the previous findings (10–12), demonstrating that NC cells contribute to the chick thyroid complex. We observed GFP-positive cells extensively surrounding the anlagen of individual glands and contributing to the mesenchymal cells of the thyroid, parathyroid, and ultimobranchial bodies (Fig. 1, E and F). Moreover, it has been shown that ablation of the NC in chick causes abnormal thyroid development, resulting in a single rather than bilobed thyroid gland (12). Together, these results suggest an important role for NC cells in thyroid development.

The evolutionary origin of the thyroid gland has generally been thought to be linked to the endostyle, an endodermal evolutionary novelty of chordates (1, 15–17). This proposed connection is based on several factors, including the fact that both the endostyle and thyroid develop in the ventral pharynx and share common gene signatures (17–20). Moreover, they have functional similarities in the synthesis of thyroid hormone (21–24) and the ability to bind iodine (25, 26). The endostyle is a groove-like structure along the ventral margin of the pharynx, functioning in filter feeding by producing mucus to capture food particles (1, 15, 27, 28). The basic architecture of this exocrine gland follows a symmetrical, groove-like pattern, consisting of several cell types (15, 19, 20), including glandular, supporting, and hair cells. The complexity of the endostyle increased over the course of chordate evolution. While there is a simple symmetrical groove-like endostyle in amphioxus, the endostyle becomes more elaborate in Tunicates (e.g., *Ciona*, *Oikopleura*, or *Doliopsis*) (19, 29–31) culminating in a more complex bilobed endostyle in larval lamprey (known as ammocoete; Fig. 1G), which eventually transforms into thyroid follicles in lamprey after metamorphosis (Fig. 1H). Thus, the trajectory of endostyle elaboration in the chordate lineage supports a possible evolutionary linkage to the thyroid. As a member of an early branching lineage, the (jawless) lamprey holds a critical phylogenetic position in the vertebrate tree of life and is relevant to our understanding of the evolution of vertebrate

¹Division of Biology and Biological Engineering, California Institute of Technology, Pasadena, CA 91125, USA. ²South Bohemian Research Center of Aquaculture and Biodiversity of Hydrocenoses, Faculty of Fisheries and Protection of Waters, University of South Bohemia in Ceske Budejovice, Vodnany, 38925, Czech Republic. ³Department of Organismal Biology, Uppsala University, Uppsala, SE75236, Sweden. ⁴Department of Zoology, Faculty of Science, Charles University in Prague, Prague, 12800, Czech Republic.

*Corresponding author. Email: jstundl@caltech.edu (J.S.); mbronner@caltech.edu (M.E.B.)

†These authors contributed equally to this work.

‡Present address: Department of Biology, Duke University, Durham, USA.

§Present address: Department of Molecular and Cell Biology, University of California, Berkeley, USA.

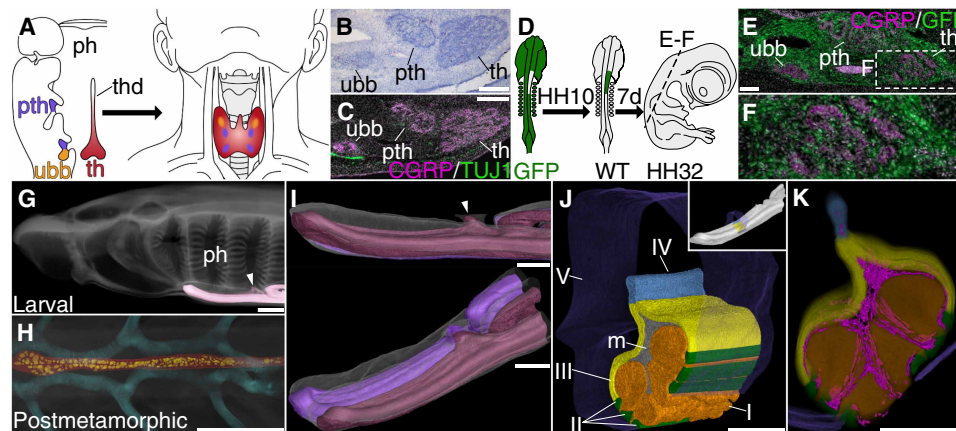


Fig. 1. Development of the lamprey endostyle. (A) Diagram illustrating the development of the mammalian thyroid (red) from the pharyngeal floor and its fusion with other endocrine organs, including the parathyroid (purple) and ultimobranchial bodies (orange). (B and C) Sagittal sections of an HH32 chick embryo showing the thyroid complex, composed of the thyroid, parathyroid, and ultimobranchial bodies. TUJ1 (green; neuronal marker) and CGRP (magenta; calcitonin gene-related peptide) immunoreactivity in HH32 embryo. (D) Schematic diagram of a unilateral isotopic grafting experiment in which GFP-positive dorsal neural tube tissue is transplanted into wild-type (WT) chick embryos (HH10) and analyzed at stage HH32. (E and F) Coronal section showing GFP-positive cells contributing to the thyroid of a chick embryo at stage HH32. (G) Lateral three-dimensional (3D) rendering of the lamprey endostyle (pink), illustrating its location within the ammocoete pharyngeal region. Arrowhead indicates the position of the duct connecting the endostyle to the pharynx. (H) Ventral 3D rendering of adult thyroid follicles (yellow, in the red thyroid) in the context of branchial basket cartilages (blue) (fig. S1E). (I) 3D rendering of the bilobed lamprey endostyle with an endostylar duct (arrowhead). (J) 3D rendering of one endostyle segment (highlighted in the inset) showing the distribution of distinct cell types (I to V) and mesenchyme (m), with each color representing a different cell type (fig. S1C). (K) Rendering of blood vessels (magenta), in the endostyle. ph, pharyngeal region; pth, parathyroid; th, thyroid; thd, thyroglossal duct; ubb, ultimobranchial bodies. Scale bars: 100 μm (E), 200 μm [(B) and (C)], 150 μm [(J) and (K)], 500 μm (I), and 1500 μm [(G) and (H)].

features. The endostyle of larval lampreys may thus represent a transitional phase in the evolutionary history of the thyroid gland development from an (originally) exocrine (15, 32, 33) to an endocrine structure (5, 16, 34). Here, we investigate the lineage contribution of NC cells to the larval lamprey endostyle and possible functional role in its morphogenesis.

RESULTS

Development of the lamprey endostyle

The lamprey endostyle develops as an elongated, bilobed organ located beneath and along the pharyngeal floor (Fig. 1G, fig. S1, and movies S1 and S2), with its posterior medial end rolling upward and coiling (Fig. 1I). It connects to the pharyngeal cavity via a single duct (Fig. 1, G to I), which is likely homologous to the mammalian thyroglossal duct (24). After metamorphosis, the endostyle transforms into thyroid follicles of varying diameters, located beneath the tongue musculature (Fig. 1H and fig. S1). The prospective endostyle begins to invaginate from the pharyngeal floor during early development (fig. S4) and subsequently differentiates into several morphologically distinct cell types and becomes fully differentiated at the T30 stage (early ammocoete) (Fig. 1J and movie S2) (35, 36). The glandular cells (type I), organized into four large, fan-shaped bundles, are surrounded by mesenchymal cells (Fig. 1J) and blood vessels (Fig. 1K). The other cell types in the endostylar epithelium (types II to IV) are intermingled, while the last cell type (type V) lines the endostylar lumen and forms the median septum (Fig. 1J and fig. S1). After metamorphosis, the ammocoete endostyle undergoes a complete restructuring, with only two cell types (II and III) contributing to the formation of the adult thyroid follicles (Fig. 1H and fig. S1) (35, 37).

Developmental program of lamprey endostyle

To gain a better understanding of the molecular machinery driving lamprey endostyle development, we dissected endostyles from post-latching and larval stages (T27 to T30) (36) and performed bulk RNA sequencing (RNA-seq). Because of the high similarity in gene expression between the vertebrate thyroid and chordate endostyle (18–20, 38, 39), we identified up-regulated genes associated with endostyle morphogenesis [*Pax2/5/8*, *Hhex*, *Ttf1* (also known as *Nkx2.1*), etc.] and differentiation (*Tpo*, *Duox1*, *TG*, *Slc26a4*, *Slc5a5*, etc.) (Fig. 2A). Most of these genes were common to both structures, with exception of *Slc5a5*, which has not previously been reported to be expressed in the endostyle. These data demonstrate that a similar genetic toolkit involved in thyroid development, and differentiation (38, 39) is also present during morphogenesis of the lamprey endostyle (Fig. 2A and fig. S2). On the basis of a high transcriptome similarity, this suggests potential homology of these pharyngeal-derived organs.

Next, we used highly sensitive hybridization chain reaction (HCR) to analyze the expression of these thyroid-associated genes and identify the specific cell types in which they are expressed (Fig. 2, B to E, and fig. S3). HCR reveals first detectable colocalization of several of these markers (*Pax2/5/8*, *Hhex*, and *Ttf1*) at stage T25 (fig. S4), preceding differentiation of the endostyle. The most notable genes are *Tpo* (thyroid peroxidase) and *Duox1* (dual oxidase 1), which play key roles in the functional differentiation of the thyroid and are essential for thyroid hormone synthesis (18, 39). The data show that their expression in the lamprey endostyle is exclusively confined to cell types II and III (Fig. 2E and fig. S3), which are proposed to be thyroid-like cells that contribute to the formation of adult thyroid follicles. KEGG (Kyoto Encyclopedia of Genes and Genomes) pathway mapping identified a large number of up-regulated genes involved in thyroid biosynthetic processes at stage T30 (fig. S5), further

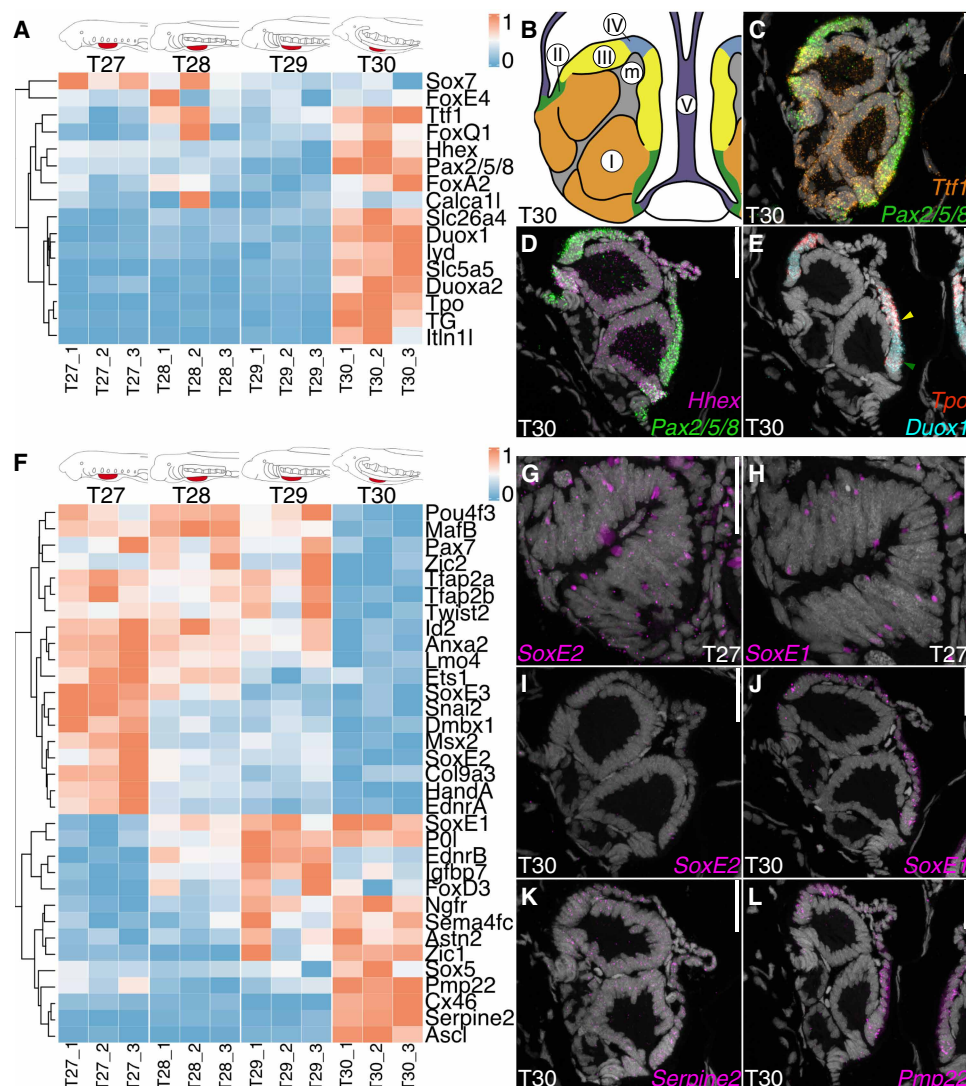


Fig. 2. Developmental program of lamprey endostyle. (A) Heatmap showing differentially expressed candidate genes ($P \leq 0.05$) associated with thyroid and chordate endostyle development from T27 to T30. (B) Diagram illustrating individual endostylar cell types in different colors. (C to E and G to L) Transverse sections demonstrating expression of candidate genes in left half of the endostyle at stage T30 (C to E and I to L) and T27 (G and H). Arrowheads indicate expression in cell type II (green) and type III (yellow), which give rise to adult lamprey thyroid after metamorphosis from ammocoete. In (G) and (H), the endostylar cells contain the highly autofluorescent yolk pellets present in most cells at stage T27. (F) Heatmap showing differentially expressed candidate genes ($P \leq 0.05$) associated with NC GRN, including SCP from T27 to T30. Scale bars, 10 μm (I) and 25 μm [(C) to (E), (G) and (H), and (J) to (L)].

supporting previous evidence that the lamprey endostyle has the capacity to synthesize thyroid hormones (22, 24) and suggesting that this capability may already be present before metamorphosis into thyroid follicles. In the context of data from nonvertebrate chordates (19, 20), these findings further support a potential homology between the vertebrate endocrine thyroid gland and the exocrine chordate endostyle.

Since the thyroid is formed not only from the endoderm but may also involve the participation of NC cells in amniotes (10–12, 14), we explored the transcriptional profiles of genes associated with the NC gene regulatory network (GRN) (40). During early endostyle development, we observed enrichment of embryonic NC genes such as *SoxE3*, *SoxE2*, and *Ets1* (Fig. 2F). Some of these genes are also involved in branching morphogenesis—a process that efficiently increases the surface area with minimal volume expansion, as seen in the development

of lungs or ocular glands (41, 42). As endostyle development progresses, the expression of embryonic NC genes is down-regulated, while genes associated with Schwann cell precursors (SCPs), such as *Pmp22*, *Serpine2*, and *Cx46* (43), become enriched (Fig. 2, F to L). SCPs are glial progenitors derived from NC and have broad developmental potential as embryonic NC cells (44). These cells express a characteristic transcriptional signature of *Sox8*, *EndrB*, and *Serpine2* (43). A similar signature is also displayed in the developing lamprey endostyle (Fig. 2F and fig. S6). Together, these results indicate that NC GRN genes are active during endostyle formation.

NC participates in endostyle development

Given the strong NC GRN signatures, we next tested a possible NC contribution to the lamprey endostyle in vivo. To this end, we performed lineage tracing experiments using cell tracker CM-DiI

injected into the forming neural tube (Fig. 3, A and B) and followed subsequent development of the embryo and up to early stage T30, when the lamprey first becomes an ammocoete larvae with a fully differentiated endostyle. Five days postinjection, we observed NC cells populating the pharyngeal arches (Fig. 3, C and D), following previously well-described NC migratory pathways (45, 46). At stage T30, the CM-Dil-positive cells were observed in cartilages of the branchial basket and in the endostyle (Fig. 3, E to G). The CM-Dil-positive cells contributed to various parts of the endostyle, including all cell types except for the glandular cells of type I (Fig. 3, H to M). While most CM-Dil-positive cells were found in the endostylar mesenchyme (Fig. 3M) and cell type V, forming the median septum and the wall (Fig. 3L), some labeled cells were also present among the thyroid-like cell types II and III (Fig. 3, I and J, and fig. S7).

To test whether the CM-Dil-positive cells are thyroid like, we performed HCR for genes exclusively expressed in these cell types II and III, such as *Duox1* (Fig. 2E and fig. S7). Our results demonstrate that *Duox1* expression overlaps with CM-Dil-positive cells (Fig. 3N), suggesting that the NC contributes to the development of thyroid-like domain.

NC controls proper endostyle development

Given that our lineage tracing revealed a NC contribution to the endostyle, we next asked whether these NC-derived cells play a functional role in endostyle formation. To test this, we optimized a method for multiplexed CRISPR-Cas9-mediated mutagenesis in lamprey and used it to disrupt several genes associated with the NC GRN: *Tfap2a*, *FoxD3*, *SoxE2*, and *SoxE3* (Fig. 4, A to C, and fig. S8).

Simultaneous targeting of *Tfap2a* and *FoxD3* in zebrafish generates mutants lacking nearly all NC derivatives (47, 48). After mutation of these genes in lamprey, we observed reductions in melanophores, which appear less dendritic and more punctate—a hallmark of dying melanocytes. However, the most apparent NC-related phenotype was associated with the oropharyngeal region, including a hypomorphic branchial basket (Fig. 4B and figs. S8 and S9) and misshapen cranial ganglia (fig. S8). Loss of *Tfap2a* and *FoxD3* also reduces the size of the endostyle [compare Fig. 4 (A to Ac) and Fig. 4 (B to Bc)]. To analyze these crispants in more detail, we performed HCR against *Duox1* and *Tpo*, along with histological analysis. Our data reveal severe anomalies in endostyle bilateralization, with only a single lobe, fused in the midline, rather than forming two lobes (Fig. 4, B to Bc, and fig. S8). This morphology is highly reminiscent of the effects of NC ablation on thyroid development (12). In addition, NC mutagenesis led to severe disruptions in endostyle structure, with glandular (type I) and other cell types (II to V) failing to form properly (Fig. 4, B to Bc). *SoxE2* and *SoxE3* crispants exhibited a phenotype highly similar to that of the *Tfap2a/FoxD3* double crispants described above (Fig. 4, C to Cc, and figs. S8 and S9). Loss of NC cells in all of these crispants resulted in down-regulation of *Duox1* expression (Fig. 4 and fig. S8), suggesting that *Duox1* may function as a downstream effector gene or may be due to a developmental lag, as *Duox1* is normally expressed later during development (fig. S3).

Together, our results indicate that the NC plays a crucial role in the proper morphogenesis of the lamprey endostyle, including the differentiation of individual cell types and the formation of a bilobed organ. These findings align with evidence from chick embryos, where

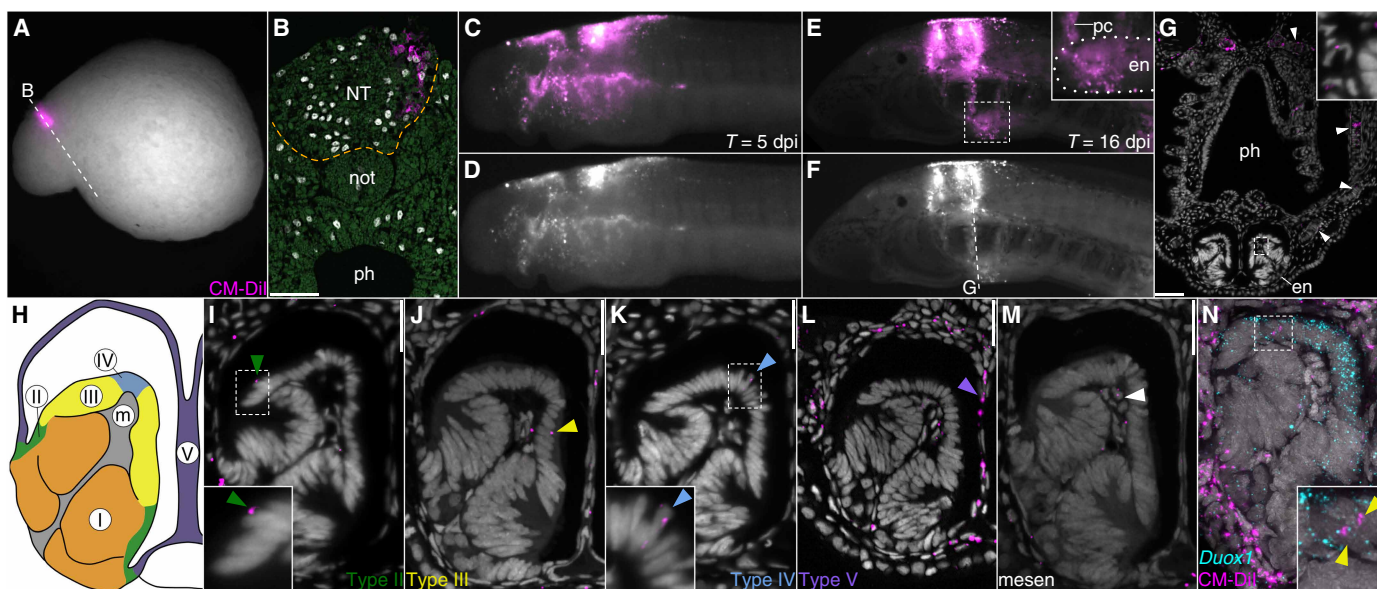


Fig. 3. NC participates in endostyle development. (A) Lateral view of embryo at stage T21 demonstrating the location of CM-Dil injection. (B) Transverse section showing the location of CM-Dil labeling only in the neural tube (demarcated dashed line). (C and D) CM-Dil-positive cranial NC cells migrating ventrally from the neural tube at 5 days postinjection (dpi). (E and F) At 16 dpi, CM-Dil-positive cells populating the endostyle (detailed view in the inset). (G) Transverse section reveals the distribution of CM-Dil-positive cells within expected NC derivatives, such as cartilage of the branchial basket (white arrowheads) and the endostyle (inset). (H) Diagram illustrating individual endostylar cell types in different colors. (I to M) Transverse sections show CM-Dil-positive NC cells (corresponding-colored arrowheads) in endostyle cell types (II to V) and the mesenchyme. Insets show higher magnification of CM-Dil-positive cell in both cell types II and IV. Note that each image corresponds to a different experimental individual. (N) Transverse section shows CM-Dil signal (magenta) overlapping with HCR expression of *Duox1* (cyan) in two cells of type III (yellow arrowheads). en, endostyle; not, notochord; NT, neural tube; pc, pharyngeal cartilage; ph, pharynx. Scale bars, 25 μ m [(I) to (N)] and 50 μ m [(B) and (G)].

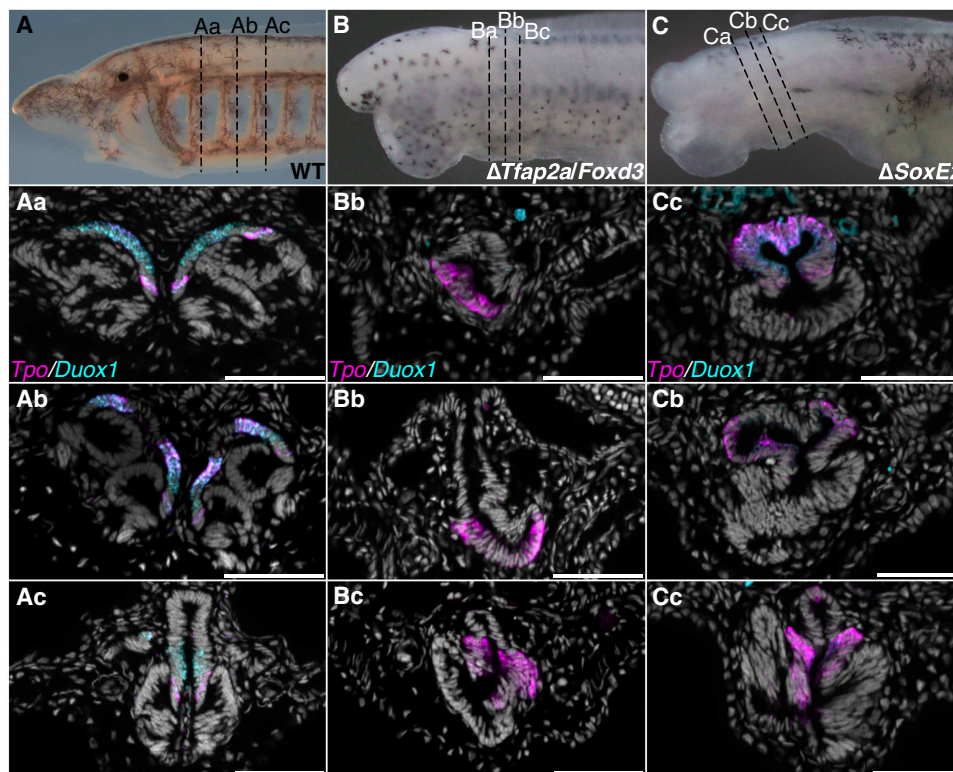


Fig. 4. NC controls proper endostyle development. (A to C) Lateral view of the lamprey head of WT (A), *Tfap2a/Foxd3* (B), and *SoxE2* (C) crispant at stage T30. (Aa to Cc) Transverse sections in the anterior (Aa to Ca), middle (Ab to Cb), and posterior (Ac to Cc) parts of the endostyle demonstrating its morphology and spatial expression of *Duox1* (cyan) and *Tpo* (magenta) genes encoding enzymes related to thyroid. Both these genes are exclusively expressed in endostylar cell types II and III which give rise to adult lamprey thyroid. The position of individual sections is highlighted by dashed lines. Scale bars, 50 μm (Aa to Cc).

NC ablation leads to the development of hypoplastic or aplastic pharyngeal-derived endocrine glands, including the thymus, parathyroids, and thyroid (11, 12).

DISCUSSION

The evolutionary origin of the vertebrate thyroid has been a subject of recent controversy. Potential homology between the nonvertebrate chordate endostyle and the vertebrate thyroid was first proposed over a century ago based on shared endodermal origins (2, 15, 16) and further supported by endostyle's ability to bind iodine and synthesize thyroid hormones (24, 25, 49, 50). Since the metamorphosing lamprey breaks up the endostyle into a series of thyroid follicles, lampreys have been considered as a good model and evolutionary bridge for understanding the origin of the thyroid gland. However, this idea has been challenged by recent paleontological evidence from direct-developing Paleozoic stem lampreys that apparently lack a larval stage and do not have an identifiable endostyle (51). On this basis, the authors suggest that the endostyle of extant lampreys may represent a derived state that arose either by convergent evolution or reversal [but see the commentary (52) for a contrary opinion].

Here, we tackle the question about the developmental origin of the lamprey endostyle by analyzing the extant lamprey endostyle using gene profiling, lineage tracing, and functional analysis. Our transcriptomic and expression data revealed that genes generally associated with thyroid development, including those involved in thyroid hormone

synthesis (Fig. 2 and figs. S2 to S5), are expressed in the developing and differentiating lamprey endostyle. This supports the previously proposed hypothesis that the 'thyroid developmental program' is conserved among chordates. Thus, the lamprey endostyle functions as both an exocrine and endocrine organ.

While the lamprey endostyle uses a conserved genetic program, its development differs notably from that of nonvertebrate chordates like amphioxus or *Ciona*. Rather than forming a simple groove-like structure, the lamprey endostyle develops into a complex, bilobed organ composed of several cell types (Fig. 1), including cells that give rise to thyroid follicles of adult lampreys. This raises the question of whether the lamprey endostyle, like the chick thyroid, has a dual origin from both endoderm and NC. Our transcriptomic profiling of the lamprey endostyle revealed highly up-regulated genes associated with the embryonic NC GRN as well as genes connected with NC-derived Schwann cells and their precursors (Fig. 2 and fig. S6), including "hub" genes like *Sox8*, *EdnrB*, or *Serpine2* (43). Consistent with this, our lineage tracing reveals a NC contribution to various cell types within the endostyle, including prospective thyroid cells (Fig. 3). Since the NC likely co-opted developmental programs typically characteristic of other germ layers to give rise to cell types such as osteoblasts or cardiomyocytes (53), an intriguing possibility is that it might also contribute to endostylar epithelial cells. Given that our CM-DiI labeling revealed a relatively small number of DiI staining in type II/III epithelial cells, a NC contribution to these cells remains inconclusive. This may be due to proliferative

dilution of the dye during development. In gnathostomes, only the mesenchymal, but not epithelial, components of “the thyroid complex” are NC derived (14, 54). Resolution of this question will require the advent of new lineage techniques that are now unavailable in lamprey.

Given that SCPs are multipotent, capable of giving rise to different cell types like enteric neurons (55), odontoblasts (56), carotid body cells (57), and neuroendocrine cells (58), we speculate that the NC cells and NC-derived SCPs may play a role in the differentiation of the endostyle (fig. S6). They also may facilitate elaboration of the gland, given that NC-associated genes, such *SoxE* genes, have been implicated in branching morphogenesis (41, 42). Nevertheless, the expression of *SoxE* genes and other NC GRN genes supports the hypothesis that the NC cells contribute to endostyle development in lampreys. These cells may promote endostyle growth and branching, similar to their role in the branching of salivary gland epithelia (59). Whether NC cells contribute to the prospective thyroid follicles in adult lampreys remains an open question, since we cannot follow these cells into adulthood given the length to the lamprey life cycle [>7 years to maturity (27)].

We propose that the NC contribution to the developing endostyle and integration of the NC developmental program may reflect a key evolutionary step that facilitated the transition from the endostyle to thyroid gland (Fig. 5). Previous studies have demonstrated that NC ablation results in abnormal thyroid development, producing a single-lobed rather than bilobed thyroid structure (12). We observed a similar phenotype in NC crispants, which develop an incomplete endostyle with only a single lobe (Fig. 4). While it is tempting to speculate that these simplified structures are reminiscent of the

nonvertebrate chordate endostyles of amphioxus and ascidians, we cannot rule out the possibility that this severe phenotype may be secondary to other craniofacial abnormalities caused by the absence of the NC. For example, lack of NC could alter the pharyngeal region which may in turn affect branching morphogenesis of endostyle. In either scenario, our findings raise the intriguing possibility that integration of NC into the endostyle developmental program may reflect an important evolutionary step in thyroid development and particularly in the formation of a bilobed gland (Fig. 5).

MATERIALS AND METHODS

Animal husbandry

Sea lamprey (*Petromyzon marinus* Linnaeus, 1758) husbandry, gamete collections, and in vitro fertilizations were carried out as described previously (60). Adult lampreys were obtained from the US Geological Survey (USGS) Hammond Bay Biological Station, MI, USA. All the husbandry and experiments were in accordance with California Institute of Technology Institutional Animal Care and Use Committee protocol #IA23-1436. Lamprey development was staged as previously described by Tahara (36).

Grafting experiments

To trace the fate of NC cells, homotopic unilateral NC grafts were performed in ovo on chick embryos from a transgenic GFP donor to a wild-type (WT) host. WT eggs were obtained from Rhode Island Red hens (Petaluma Farm), and transgenic cytoplasmic GFP eggs were obtained from Susan Chapman (Clemson University) (61). Unilateral premigratory cardiac NC (from the level of the mid-otic

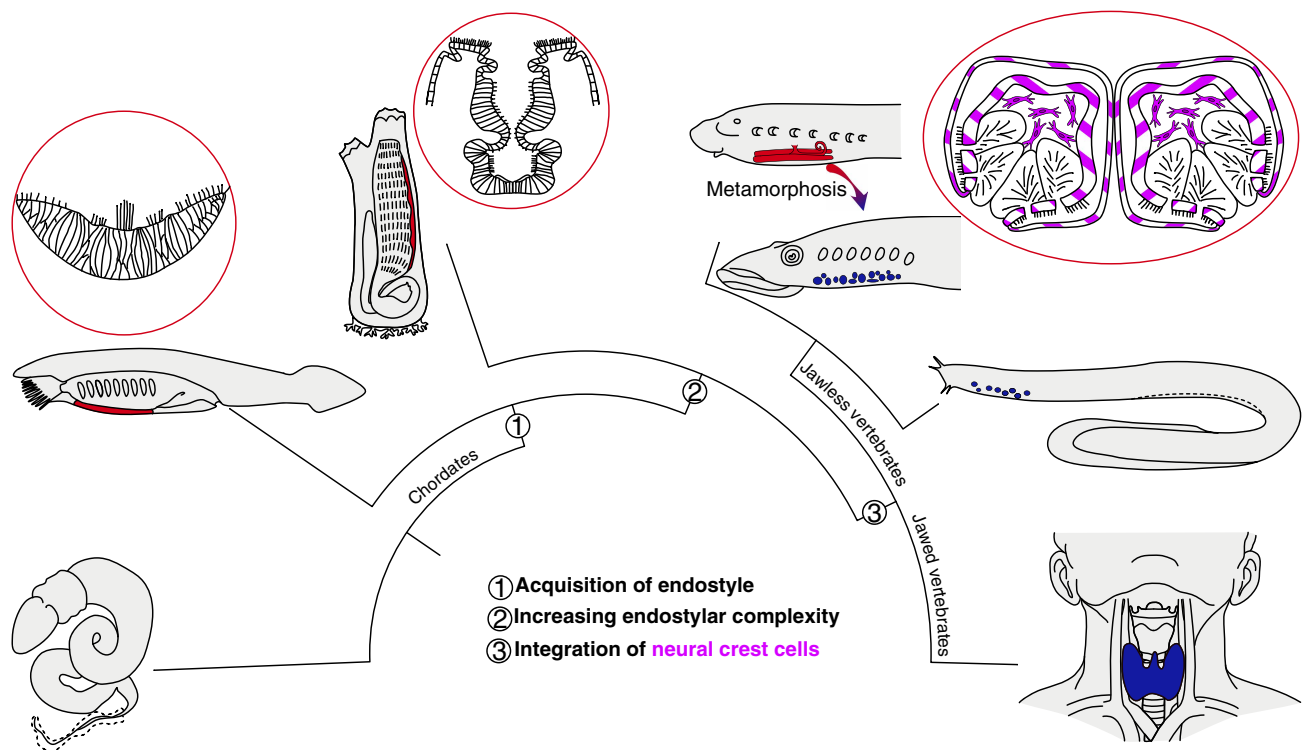


Fig. 5. Proposed model of endostyle-to-thyroid evolution. A simplified evolutionary scenario in deuterostomes, highlighting key aspects of chordate endostyle evolution and the subsequent integration of NC cells, which may have promoted thyroid evolution and bilateralization in vertebrates. The endostyle is shown in red, and the thyroid follicles/thyroid is shown in blue.

placode to the caudal limit of somite three) was first cut out using a pulled glass needle and then removed from the HH10 host. The equivalent region from a stage-matched GFP donor was cut out, transplanted, and inserted into the WT host, maintaining rostro-caudal and medio-lateral orientation. The egg was then sealed with tape and incubated (38°C) in a humidified incubator for 7 days, until the embryo reached stage HH32. Embryos were fixed in 4% paraformaldehyde (PFA) before being processed for embedding in gelatin for cryo-sectioning (16 μ m). Following sectioning, some slides from grafted or WT embryos were processed for immunohistochemistry. Primary antibodies used are as follows: rabbit anti-CGRP (#14959, Cell Signaling), 1:400; mouse anti-TUJ1 immunoglobulin G2a (#801201, BioLegend), 1:500; and goat anti-GFP (#600-101-215, Rockland), 1:500. Secondary antibodies used are as follows: donkey anti-rabbit 647 (#A31573, Invitrogen), 1:1000; donkey anti-mouse 488 (#A21202, Invitrogen), 1:1000; and donkey anti-goat 488 (#A11055, Invitrogen), 1:000. Following antibody staining, slides were mounted using Fluoromount-G (#0100-01, Southern Biotech) and imaged using a Zeiss Imager MZ with an ApoTome module. Other slides were processed for histology using hematoxylin and eosin (H&E; MHS32 and HT110216, Sigma-Aldrich). Following H&E staining, slides were mounted using DPX (distyrene, plasticizer, and xylene) mounting medium (#44581, Fluka) and imaged using a Zeiss imager MZ with a color camera.

Iodine-enhanced propagation phase-contrast synchrotron radiation microcomputed tomography

The ammocoete and postmetamorphic specimens were fixed in PFA-Carnoy before being transferred to 1 \times phosphate-buffered saline (PBS) and gradually dehydrated to 100% ethanol. They were then stained for 1 day in a solution of 1% iodine in 100% ethanol, transferred to 96% ethanol, and subsequently scanned at the beamline BM05 of the European Synchrotron Radiation Facility—Extremely Brilliant Source (ESRF-EBS) in Grenoble, France. Diffusible iodine-based contrast enhancement and propagation phase-contrast synchrotron radiation microcomputed tomography associated with the hierarchical phase-contrast tomography (HiP-CT) protocol developed by Walsh *et al.* (62) was performed following the methodology previously described by Leyhr *et al.* (63). Briefly, for scans with 3- μ m voxel size, the specimens were placed at a propagation distance of 1.45 m from the detector to maximize the phase-contrast effect. The beam was filtered with 2.3 mm of aluminium and 8 (5-mm thick) bars of silicon dioxide, thereby providing a resulting detected average energy of 78 keV. For the submicron-resolution configuration, i.e., 0.727- μ m voxel size, the detector was placed at 180 mm from the sample. The beam was filtered with 2.3 mm of aluminium, thereby providing a detected average energy of 35 keV. Reconstructed jp2000 image stacks were imported into VGStudio MAX (v2023.3, Volume Graphics, Germany) for manual segmentation and rendering at Uppsala University. The individual cell types were segmented on the basis of their morphology, as done in previous studies using classical histology (24, 35). The datasets presented in this study can be found in the following online repository hosted by the ESRF-EBS: doi.org/10.15151/esrf-dc-1966164174.

Library preparation, sequencing, and gene enrichment analysis

The individual endostyles were dissected using a microknife (0.2 mm; Fine Science Tools) and preserved in RNAlater (Sigma-Aldrich). For bulk RNA-seq, total RNA was isolated (each replicate contained

five dissected endostyles) using the RNAqueous kit (Ambion), measured by Qubit, and assessed using the Agilent bioanalyzer. The RNA-seq was performed at the Millard and Muriel Jacobs Genetics and Genomics Laboratory (California Institute of Technology, Pasadena, CA, USA) at 50 million, 50-bp, single-ended reads on three biological replicates. The libraries were built according to Illumina Standard Protocols. SR50 sequencing was performed in a HiSeq2500 Illumina sequencer. Reads were mapped to the lamprey genome assembly (kPetMar1.0) in the Stowers Institute SIMRBASE (<https://simrbase.stowers.org/sealamprey?pane=resource-1>) using Bowtie2 (64). Transcript counts were calculated using featureCounts (65). The differential gene expression analysis was performed using DESeq2 (66) in R, and statistically significant differentially expressed genes were identified globally based on an adjusted *P* value threshold of ≤ 0.05 . Candidate genes associated with thyroid/endostyle formation (18–20, 38, 39) and the NC GRN (40) were then specifically screened for their significant expression. KEGG (67) pathway mapping was performed by labeling the human orthologs of up-regulated lamprey genes from the aforementioned RNA-seq dataset to TRH-TSH-TH signaling (nt06322). The RNA-seq data reported in this paper have been deposited in the National Center for Biotechnology Information Gene Expression Omnibus database (accession no. GSE294220).

Multispecies analysis

The Zebrafish *Pax2a*-High/Low thyrocyte dataset (accession no. GSE153197) (68) and the *Ciona intestinalis* endostyle dataset (accession no. SRR14597460) (69) were downloaded from National Center for Biotechnology Information—SRA database. Zebrafish-human gene orthology data were downloaded from The Zebrafish Information Network (ZFIN) (<https://zfin.org/downloads>). *Ciona*-human and lamprey-human gene orthology was performed using orthofinder (70) following default parameters. FASTQ files were aligned to their respective genomes—*Danio rerio* GRCz11 and *C. intestinalis* GCF_000224145.3_KH using the Bowtie2 aligner. Transcript counts were calculated using featureCounts, and differential gene expression analysis was performed using DESeq2 after correcting for batch effect using Combat-seq (71). A total of 1673 gene orthologs common to *Ciona*, lamprey, and zebrafish were incorporated in the analysis to plot the heatmap. Similarly, 5923 gene orthologs were used for generating the heatmap of transcriptome comparison between lamprey and zebrafish.

Hybridization chain reaction

HCR v3.0 was performed according to the protocol suggested by Molecular Technologies (72) for zebrafish with several modifications. Briefly, methanol-fixed tissues were rehydrated by series of methanol/PBS-Tween (PBST) solutions (2 \times 100, 75, 50, and 25%; every step 5 min), washed in PBST (2 \times 5 min), treated with proteinase K (20 mg/ml; time depends on developmental stage, e.g., 30 min for T30), washed in PBST, washed in 0.1 M triethanolamine (quick wash, 3 and 5 min), incubated in 0.25 and 50% acetic anhydride in 0.1 M triethanolamine (each step 12 min), washed in PBST (2 \times 5 min), postfixed in 4% PFA (10 min), washed in PBST (3 \times 5 min), prehybridized in 30% probe hybridization buffer at 37°C (60 min), and incubated with probes (usually 2 μ l of 2 μ M stock per probe mixture) in probe hybridization buffer at 37°C overnight. All probes were generated by and ordered through Molecular Technologies (<https://www.moleculartechnologies.org>). Probes were designed against

P. marinus Pax2/5/8 (XM_032949689.1), *Hhex* (XM_032952123.1), *Ttf1* (LOC116943240), *Duox1* (XM_032947354.1), *Tpo* (XM_032959598.1), *SoxE2* (DQ328983.1), *SoxE1* (XM_032961232), *Pmp22* (PMZ0041331-RA), and *Serpine2* (XM_032958326.1). After HCR, the hybridized samples were mounted into JB-4 resin [followed the manufacturer's instructions and as described by Stundl *et al.* (73)], sectioned (5 to 7 μm), and counterstained with Fluoroshield with 4',6-diamidino-2-phenylindole (DAPI; Sigma-Aldrich). HCR on sections was performed according to the protocol suggested by Molecular Technologies (72) and Criswell and Gillis (74). Instead of using paraffin sections, the samples were embedded in low-melting agarose and transferred through a series of sucrose solutions into OCT. The sucrose concentrations used were 5, 15, and 30%, followed by a 1:1 mixture of 30% sucrose and OCT, and lastly 100% OCT. This embedding approach preserved tissue integrity, and the OCT blocks were sectioned at 14 μm . Images were taken with Zeiss AxioImager.M2 equipped with an Apotome.2 or with a confocal microscope LSM 900.

CM-Dil lineage tracing

The lamprey embryos at stage T21 (36) were manually dechorionated and positioned in suitable hollows in petri dishes with agarose. Cell tracker CM-Dil (1,1'-diiododecyl-3,3,3'-tetramethylindocarbocyanine perchlorate) was prepared as was described previously by Stundl *et al.* (73) and injected as described by Häming *et al.* (75). The microcapillaries (Quartz, I.D.: 0.70) were prepared in a Sutter Instruments P-2000 puller. Injected embryos were kept individually in the 96-well plates with agarose containing 1 \times Marc's Modified Ringer's solution (MMR) at 16°C and grown to T30 stage (36). Individuals were screened for CM-Dil-positive labeling, euthanized using an overdose of tricaine (MS-222), and fixed in 4% PFA at 4°C overnight. In total, we successfully injected 73 embryos and fixed as a control of properly performed injection immediately after the injection ($n = 10$), 5 days postinjection ($n = 8$), and at stage T30 ($n = 55$; histologically analyzed 17 embryos; Fig. 3 and table S1). The individuals for histological analysis were mounted into JB-4 resin, sectioned (5 μm), and counterstained with Fluoroshield with DAPI (Sigma-Aldrich). In addition, we used four CM-Dil-positive embryos to verify whether NC-positive cells overlap with markers that are exclusively expressed in cell types II and III, such as *Duox1* or *Tpo*, as well as *Pax2/5/8*, which is predominantly expressed in these cell types. However, we observed positive HCR staining only for *Duox1*, which may be due to the use of samples fixed with only 4% PFA (embedding for HCR on sections is described above). The cell lineage experiments were performed in six independent rounds of injections during lamprey seasons 2020, 2021, and 2022.

Immunohistochemistry

The methanol-fixed samples were rehydrated through graded methanol/PBS (2 \times 100, 75, 50, and 25%; every step 10 min) into 1 \times PBS. After three washes in 1 \times PBS (10 min each), the samples were transferred to permeabilization buffer [1 \times PBS:dimethyl sulfoxide (DMSO):10% Triton X-100; 1:1:1] for 30 min at room temperature (RT). Next, the samples were washed three times in 0.2% PBS-Triton X-100 (5 min each), permeabilized with proteinase K (10 $\mu\text{g}/\text{ml}$) for 30 min, and subsequently postfixed in 4% PFA for 20 min at RT. Samples were then equilibrated in blocking solution (10% donkey serum, 0.1% PBS-Triton X-100, 0.5% bovine serum albumin, and 1% DMSO) at RT for 90 min. Next, they were incubated with primary antibodies—anti-acetylated tubulin (#T7451, Sigma-Aldrich; 1:200) and

SOX10 (#GTX128374, GeneTex; 1:200)—diluted in blocking solution, overnight at 4°C. After washing in 0.2% PBS-TritonX-100, the samples were incubated with secondary antibodies (Alexa Fluor; 1:250), also diluted in blocking solution, overnight at 4°C. The next day, samples were washed several times in 0.2% PBS-Triton X-100, followed by a 1 \times PBS wash, and then either processed for whole-mount imaging or prepared for resin histology (CM-Dil-positive samples). For whole-mount imaging, samples were counterstained with DAPI (1:10,000 in 0.2% PBS-Triton X-100) at RT for 90 min and then cleared in refractive index matching solution (RIMS) overnight at 4°C. Last, the samples were embedded in RIMS-low-melting agarose and imaged using the LSM900.

CRISPR-Cas9 mutagenesis

Guide RNA (gRNAs) for lamprey *SoxE2*, *SoxE3*, *Tfap2a*, and *FoxD3* (table S2 and fig. S9) were designed using CRISPRscan [https://crisprscan.org/; (76)]. The gRNAs were checked for off-targets using BLAST [https://blast.ncbi.nlm.nih.gov/Blast.cgi; (77)] and ordered from Integrated DNA Technologies (https://idtdna.com/page) as CRISPR RNAs (crRNAs). We followed a recently published protocol for efficient CRISPR-Cas9 mutagenesis in zebrafish (78). Injection mixes (RNP complex mixture = Cas9 protein/crRNA:tracrRNA duplex) were prepared fresh for each injection and injected into the cytoplasm of one-cell stage lamprey embryos through the egg membrane using quartz microcapillaries. To generate F0 individuals, each lamprey embryo was injected approximately by 4 to 5 nl and kept separately in 96-well plates containing 0.05 \times MMR. Alcian blue staining was performed as previously described (79), and SOX10 antibody staining (#GTX128374, GeneTex; 1:200) was carried out as described above.

Genotyping

For the confirmation of successful mutagenesis, we genotyped the individual candidate crispants. Briefly, the genomic DNA was isolated from control and analyzed crispants according to the protocol described in ZFIN (http://zfin.org/zf_info/zfbook/chapt9/9.3.html). Target regions were amplified using genotyping primers for each gRNA (table S3), followed by the T7 endonuclease assay, and quantified by gel electrophoresis. Next, the products were purified and sent for premium polymerase chain reaction sequencing to Primordium Labs (https://primordiumlabs.com/) and analyzed by using CRISPResso2 (fig. S9) (80).

Supplementary Materials

The PDF file includes:

Figs. S1 to S9

Tables S1 to S3

Legends for movies S1 and S2

Other Supplementary Material for this manuscript includes the following:

Movies S1 and S2

REFERENCES AND NOTES

1. N. Satoh, *Chordate Origins and Evolution: The Molecular Evolutionary Road to Vertebrates* (Academic, 2016).
2. G. R. De Beer, *Vertebrate Zoology* (Sedwick & Jackson, 1928).
3. A. Grevellec, A. S. Tucker, The pharyngeal pouches and clefts: Development, evolution, structure and derivatives. *Semin. Cell Dev. Biol.* **21**, 325–332 (2010).
4. M. De Felice, R. Di Lauro, Thyroid development and its disorders: Genetics and molecular mechanisms. *Endocr. Rev.* **25**, 722–746 (2004).

5. M. Nilsson, H. Fagman, Development of the thyroid gland. *Development* **144**, 2123–2140 (2017).
6. B. A. Policeni, W. R. Smoker, D. L. Reede, Anatomy and embryology of the thyroid and parathyroid glands. *Semin. Ultrasound CT MR* **33**, 104–114 (2012).
7. Y. Kameda, Morphological and molecular evolution of the ultimobranchial gland of nonmammalian vertebrates, with special reference to the chicken C cells. *Dev. Dyn.* **246**, 719–739 (2017).
8. B. Alt, S. Reibe, N. M. Feitosa, O. A. Elsalini, T. Wendl, K. B. Rohr, Analysis of origin and growth of the thyroid gland in zebrafish. *Dev. Dyn.* **235**, 1872–1883 (2006).
9. H. Fagman, M. Nilsson, Morphogenesis of the thyroid gland. *Mol. Cell. Endocrinol.* **323**, 35–54 (2010).
10. C. S. Le Lièvre, N. M. Le Douarin, Mesenchymal derivatives of the neural crest: Analysis of chimaeric quail and chick embryos. *J. Embryol. Exp. Morphol.* **34**, 125–154 (1975).
11. D. E. Bockman, M. L. Kirby, Dependence of thymus development on derivatives of the neural crest. *Science* **223**, 498–500 (1984).
12. K. Maeda, R. Asai, K. Maruyama, Y. Kurihara, T. Nakanishi, H. Kurihara, S. Miyagawa-Tomita, Postotic and preotic cranial neural crest cells differently contribute to thyroid development. *Dev. Biol.* **409**, 72–83 (2016).
13. X. Jiang, D. H. Rowitch, P. Soriano, A. P. McMahon, H. M. Sucov, Fate of the mammalian cardiac neural crest. *Development* **127**, 1607–1616 (2000).
14. E. Johansson, L. Andersson, J. Örnros, T. Carlsson, C. Ingesson-Carlsson, S. Liang, J. Dahlberg, S. Jansson, L. Parrillo, P. Zoppoli, G. O. Barila, D. L. Altschuler, D. Padula, H. Lickert, H. Fagman, M. Nilsson, Revising the embryonic origin of thyroid C cells in mice and humans. *Development* **142**, 3519–3528 (2015).
15. R. Olsson, Endostyles and endostylar secretions: A comparative histochemical study. *Acta Zool.* **44**, 299–328 (1963).
16. W. Müller, Über die Hypobranchialrinne der Tunicaten und deren Vorhandensein bei Amphioxus und den Cyclostomen. *Jena Z. Med.* **7**, 327–332 (1873).
17. W. Takagi, F. Sugahara, S. Higuchi, R. Kusakabe, J. Pascual-Anaya, I. Sato, Y. Oisi, N. Ogawa, H. Miyaniishi, N. Adachi, S. Hyodo, S. Kuratani, Thyroid and endostyle development in cyclostomes provides new insights into the evolutionary history of vertebrates. *BMC Biol.* **20**, 76 (2022).
18. M. Ogasawara, R. Di Lauro, N. Satoh, Ascidian homologs of mammalian thyroid peroxidase genes are expressed in the thyroid-equivalent region of the endostyle. *J. Exp. Zool.* **285**, 158–169 (1999).
19. J. Hiruta, F. Mazet, K. Yasui, P. Zhang, M. Ogasawara, Comparative expression analysis of transcription factor genes in the endostyle of invertebrate chordates. *Dev. Dyn.* **233**, 1031–1037 (2005).
20. A. Jiang, K. Han, J. Wei, X. Su, R. Wang, W. Zhang, X. Liu, J. Qiao, P. Liu, Q. Liu, J. Zhang, N. Zhang, Y. Ge, Y. Zhuang, H. Yu, S. Wang, K. Chen, W. Lu, X. Xu, H. Yang, G. Fan, B. Dong, Spatially resolved single-cell atlas of ascidian endostyle provides insight into the origin of vertebrate pharyngeal organs. *Sci. Adv.* **10**, eadi9035 (2024).
21. E. J. W. Barrington, A. Thorpe, The identification of monoiodotyrosine, diiodotyrosine and thyroxine in extracts of the endostyle of the ascidian, *Ciona intestinalis* L. *Proc. R. Soc. Lond. B. Biol. Sci.* **163**, 136–149 (1965a).
22. G. M. Wright, M. F. Filosa, J. H. Youson, Light and electron microscopic immunocytochemical localization of thyroglobulin in the thyroid gland of the anadromous sea lamprey, *Petromyzon marinus* L., during its upstream migration. *Cell Tissue Res.* **187**, 473–478 (1978).
23. S. Suzuki, Y. Kondo, Thyroidal morphogenesis and biosynthesis of thyroglobulin before and after metamorphosis in the lamprey, *Lampetra reissneri*. *Gen. Comp. Endocrinol.* **21**, 451–460 (1973).
24. B. Kluge, N. Renault, K. B. Rohr, Anatomical and molecular reinvestigation of lamprey endostyle development provides new insight into thyroid gland evolution. *Dev. Genes Evol.* **215**, 32–40 (2005).
25. E. J. W. Barrington, A. Thorpe, An autoradiographic study of the binding of iodine-125 in the endostyle and pharynx of the ascidian, *Ciona intestinalis* L. *Gen. Comp. Endocrinol.* **5**, 373–385 (1965b).
26. G. Fredriksson, L. E. Ericson, R. Olsson, Iodine binding in the endostyle of larval *Branchiostoma lanceolatum* (Cephalochordata). *Gen. Comp. Endocrinol.* **56**, 177–184 (1984).
27. M. W. Hardisty, *Biology of the Cyclostomes* (Chapman and Hall, 1979).
28. M. C. Holley, Cell shape, spatial patterns of cilia, and mucus-net construction in the ascidian endostyle. *Tissue Cell* **18**, 667–684 (1986).
29. H. Fujita, H. Nanba, Fine structure and its functional properties of the endostyle of ascidians, *Ciona intestinalis*. A part of phylogenetic studies of the thyroid gland. *Z. Zellforsch. Mikrosk. Anat.* **121**, 455–469 (1971).
30. R. Olsson, The cytology of the endostyle of *Oikopleura dioica*. *Ann. N. Y. Acad. Sci.* **118**, 1038–1051 (1965).
31. P. Compère, J. E. A. Godeaux, On endostyle ultrastructure in two new species of loliolid-like tunicates. *Mar. Biol.* **128**, 447–453 (1997).
32. J. W. Moore, J. M. Mallat, Feeding of larval lamprey. *Can. J. Fish. Aquat. Sci.* **37**, 1658–1664 (1980).
33. J. Mallat, The suspension feeding mechanism of the larval lamprey *Petromyzon marinus*. *J. Zool.* **194**, 103–142 (1981).
34. E. S. Goodrich, *Studies on the Structure and Development of the Vertebrates* (Macmillan and Co., 1930).
35. D. Marine, The metamorphosis of the endostyle (thyroid gland) of ammocoetes branchialis (larval land-locked *Petromyzon marinus*) (Jordan) or *Petromyzon dorsatus* (Wilder). *J. Exp. Med.* **17**, 379–395 (1913).
36. Y. Tahara, Normal stages of development in the lamprey, *Lampetra reissneri* (Dybowski). *Zoolog. Sci.* **5**, 109–118 (1988).
37. K. N. Hausken, T. J. Marquis, S. A. Sower, Expression of two glycoprotein hormone receptors in larval, parasitic phase, and adult sea lampreys. *Gen. Comp. Endocrinol.* **264**, 39–47 (2018).
38. R. Parlato, A. Rosica, A. Rodriguez-Mallon, A. Affuso, M. P. Postiglione, C. Arra, A. Mansouri, S. Kimura, R. Di Lauro, M. De Felice, An integrated regulatory network controlling survival and migration in thyroid organogenesis. *Dev. Biol.* **276**, 464–475 (2004).
39. L. P. Fernández, A. López-Márquez, P. Santisteban, Thyroid transcription factors in development, differentiation and disease. *Nat. Rev. Endocrinol.* **11**, 29–42 (2015).
40. M. L. Martik, M. E. Bronner, Regulatory logic underlying diversification of the neural crest. *Trends Genet.* **33**, 715–727 (2017).
41. S. Liang, E. Johansson, G. Barila, D. L. Altschuler, H. Fagman, M. Nilsson, A branching morphogenesis program governs embryonic growth of the thyroid gland. *Development* **145**, dev146829 (2018).
42. Z. Chen, J. Huang, Y. Liu, L. K. Dattilo, S. H. Huh, D. Ornitz, D. C. Beebe, FGF signaling activates a Sox9-Sox10 pathway for the formation and branching morphogenesis of mouse ocular glands. *Development* **141**, 2691–2701 (2014).
43. M. E. Kastriiti, L. Faure, D. Von Ahsen, T. G. Boudierlique, J. Boström, T. Solovieva, C. Jackson, M. Bronner, D. Meijer, S. Hadjab, F. Lallemand, A. Erickson, M. Kaucza, V. Dyachuk, T. Perlmann, L. Lahti, J. Krivanek, J. F. Brunet, K. Fried, I. Adameyko, Schwann cell precursors represent a neural crest-like state with biased multipotency. *EMBO J.* **41**, e108780 (2022).
44. T. Solovieva, M. Bronner, Schwann cell precursors: Where they come from and where they go. *Cells Dev.* **166**, 203686 (2021).
45. M. L. Martik, S. Gandhi, B. R. Uy, J. A. Gillis, S. A. Green, M. Simoes-Costa, M. E. Bronner, Evolution of the new head by gradual acquisition of neural crest regulatory circuits. *Nature* **574**, 675–678 (2019).
46. T. A. Square, D. Jandzik, J. L. Massey, M. Romáček, H. P. Stein, A. W. Hansen, A. Purkayastha, M. V. Cattell, D. M. Medeiros, Evolution of the endothelin pathway drove neural crest cell diversification. *Nature* **585**, 563–568 (2020).
47. B. L. Arduini, K. M. Bosse, P. D. Henion, Genetic ablation of neural crest cell diversification. *Development* **136**, 1987–1994 (2009).
48. W. D. Wang, D. B. Melville, M. Montero-Balaguer, A. K. Hatzopoulos, E. W. Knapik, Tfap2a and Foxd3 regulate early steps in the development of the neural crest progenitor population. *Dev. Biol.* **360**, 173–185 (2011).
49. F. Monaco, M. Andreoli, A. La Posta, J. Roche, Thyroglobulin biosynthesis in a larval (ammocoete) and adult freshwater lamprey (*Lampetra planeri* B1.). *Comp. Biochem. Physiol. B* **60**, 87–91 (1978).
50. G. Holzer, Y. Morishita, J. B. Fini, T. Lorin, B. Gillet, S. Hughes, M. Tohmé, G. Deléage, B. Demeneix, P. Arvan, V. Laudet, Thyroglobulin represents a novel molecular architecture of vertebrates. *J. Biol. Chem.* **291**, 16553–16566 (2016).
51. T. Miyashita, R. W. Gess, K. Tietjen, M. I. Coates, Non-ammocoete larvae of Palaeozoic stem lampreys. *Nature* **591**, 408–412 (2021).
52. J. Mallat, Vertebrate origins are informed by larval lampreys (ammocoetes): A response to Miyashita et al., 2021. *Zool. J. Linn. Soc.* **197**, 287–321 (2023).
53. I. Adameyko, “Elaboration of fates in neural crest lineage during evolution” in *Evolving Neural Crest Cells* (CRC Press/Taylor & Francis Group, 2020), pp. 157–183.
54. J. M. Rees, K. Kirk, G. Gattoni, D. Hockman, V. A. Sleight, D. J. Ritter, È. Benito-Gutierrez, E. W. Knapik, J. G. Crump, P. Fabian, J. A. Gillis, A pre-vertebrate endodermal origin of calcitonin-producing neuroendocrine cells. *Development* **151**, dev202821 (2024).
55. W. N. El-Nachef, M. E. Bronner, De novo enteric neurogenesis in post-embryonic zebrafish from Schwann cell precursors rather than resident cell types. *Development* **147**, dev186619 (2020).
56. N. Kaucza, M. K. Shahidi, C. Konstantinidou, V. Dyachuk, M. Kaucza, A. Furlan, Z. An, L. Wang, I. Hultman, L. Ahrlund-Richter, H. Blom, H. Brismar, N. A. Lopes, V. Pachnis, U. Suter, H. Clevers, I. Thesleff, P. Sharpe, P. Ernfor, K. Fried, I. Adameyko, Glial origin of mesenchymal stem cells in a tooth model system. *Nature* **513**, 551–554 (2014).
57. D. Hockman, I. Adameyko, M. Kaucza, P. Barraud, T. Otani, A. Hunt, A. C. Hartwig, E. Sock, D. Waithe, M. C. M. Franck, P. Ernfor, S. Ehinger, M. J. Howard, N. Brown, J. Reese, C. V. H. Baker, Striking parallels between carotid body glomus cell and adrenal chromaffin cell development. *Dev. Biol.* **444**, S308–S324 (2018).
58. A. Furlan, V. Dyachuk, M. E. Kastriiti, L. Calvo-Enrique, H. Abdo, S. Hadjab, T. Chontorotzea, N. Akkuratova, D. Usoskin, D. Kamenev, J. Petersen, K. Sunadome, F. Memic, U. Marklund, K. Fried, P. Topilko, F. Lallemand, P. V. Kharchenko, P. Ernfor, I. Adameyko, Multipotent

- peripheral glial cells generate neuroendocrine cells of the adrenal medulla. *Science* **357**, eaal3753 (2017).
59. L. Chatzeli, M. Gaete, A. S. Tucker, Fgf10 and Sox9 are essential for the establishment of distal progenitor cells during mouse salivary gland development. *Development* **144**, 2294–2305 (2017).
 60. N. Nikitina, M. Bronner-Fraser, T. Sauka-Spengler, Culturing lamprey embryos. *Cold Spring Harb Protoc.* **2009**, pdb.prot5122 (2009).
 61. M. J. McGrew, A. Sherman, S. G. Lillico, F. M. Ellard, P. A. Radcliffe, H. J. Gilhooley, K. A. Mitrophanous, N. Cambray, V. Wilson, H. Sang, Localised axial progenitor cell populations in the avian tail bud are not committed to a posterior Hox identity. *Development* **135**, 2289–2299 (2008).
 62. C. L. Walsh, P. Tafforeau, W. L. Wagner, D. J. Jafree, A. Bellier, C. Werlein, M. P. Kühnel, E. Boller, S. Walker-Samuel, J. L. Robertus, D. A. Long, J. Jacob, S. Marussi, E. Brown, N. Holroyd, D. D. Jonigk, M. Ackermann, P. D. Lee, Imaging intact human organs with local resolution of cellular structures using hierarchical phase-contrast tomography. *Nat. Methods* **18**, 1532–1541 (2021).
 63. J. Leyhr, S. Sanchez, K. N. Dollman, P. Tafforeau, T. Haitina, Enhanced contrast synchrotron X-ray microtomography for describing skeleton-associated soft tissue defects in zebrafish mutants. *Front. Endocrinol. (Lausanne)* **14**, 1108916 (2023).
 64. B. Langmead, S. L. Salzberg, Fast gapped-read alignment with Bowtie 2. *Nat. Methods* **9**, 357–359 (2012).
 65. Y. Liao, G. K. Smyth, W. Shi, featureCounts: An efficient general purpose program for assigning sequence reads to genomic features. *Bioinformatics* **30**, 923–930 (2014).
 66. M. I. Love, W. Huber, S. Anders, Moderated estimation of fold change and dispersion for RNA-seq data with DESeq2. *Genome Biol.* **15**, 550 (2014).
 67. H. Ogata, S. Goto, K. Sato, W. Fujibuchi, H. Bono, M. Kanehisa, KEGG: Kyoto encyclopedia of genes and genomes. *Nucleic Acids Res.* **27**, 29–34 (1999).
 68. P. Gillotay, M. Shankar, B. Haerlingen, E. Sema Elif, M. Pozo-Morales, I. Garteizgogea, S. Reinhardt, A. Kränkel, J. Bläsche, A. Petzold, N. Ninov, G. Kesavan, C. Lange, M. Brand, A. Lefort, F. Libert, V. Detours, S. Costagliola, S. Sumeet Pal, Single-cell transcriptome analysis reveals thyrocyte diversity in the zebrafish thyroid gland. *EMBO Rep.* **21**, e50612 (2020).
 69. S. Matsubara, T. Osugi, A. Shiraishi, A. Wada, H. Satake, Comparative analysis of transcriptomic profiles among ascidians, zebrafish, and mice: Insights from tissue-specific gene expression. *PLOS ONE* **16**, e0254308 (2021).
 70. D. M. Emms, S. Kelly, OrthoFinder: Phylogenetic orthology inference for comparative genomics. *Genome Biol.* **20**, 238 (2019).
 71. Y. Zhang, G. Parmigiani, W. E. Johnson, ComBat-seq: Batch effect adjustment for RNA-seq count data. *NAR Genom. Bioinform.* **2**, lqaa078 (2020).
 72. H. M. T. Choi, M. Schwarzkopf, M. E. Fornace, A. Acharya, G. Artavanis, J. Stegmaier, A. Cunha, N. A. Pierce, Third-generation in situ hybridization chain reaction: Multiplexed, quantitative, sensitive, versatile, robust. *Development* **145**, dev165753 (2018).
 73. J. Stundl, M. L. Martik, D. Chen, D. A. Raja, R. Franěk, A. Pospisilova, M. Pšenička, B. D. Metscher, I. Braasch, T. Haitina, R. Cerny, P. E. Ahlberg, M. E. Bronner, Ancient vertebrate dermal armor evolved from trunk neural crest. *Proc. Natl. Acad. Sci. U.S.A.* **120**, e2221120120 (2023).
 74. K. E. Criswell, J. A. Gillis, Resegmentation is an ancestral feature of the gnathostome vertebral skeleton. *eLife* **9**, e51696 (2020).
 75. D. Häming, M. Simoes-Costa, B. Uy, J. Valencia, T. Sauka-Spengler, M. Bronner-Fraser, Expression of sympathetic nervous system genes in Lamprey suggests their recruitment for specification of a new vertebrate feature. *PLOS ONE* **6**, e26543 (2011).
 76. M. A. Moreno-Mateos, C. E. Vejnár, J. D. Beaudoin, J. P. Fernandez, E. K. Mis, M. K. Khokha, A. J. Giraldez, CRISPRscan: Designing highly efficient sgRNAs for CRISPR-Cas9 targeting in vivo. *Nat. Methods* **12**, 982–988 (2015).
 77. S. F. Altschul, W. Gish, W. Miller, E. W. Myers, D. J. Lipman, Basic local alignment search tool. *J. Mol. Biol.* **215**, 403–410 (1990).
 78. F. Kroll, G. T. Powell, M. Ghosh, G. Gestri, P. Antinucci, T. J. Hearn, H. Tunbak, S. Lim, H. W. Dennis, J. M. Fernandez, D. Whitmore, E. Dreosti, S. W. Wilson, E. J. Hoffman, J. Rihel, A simple and effective F0 knockout method for rapid screening of behaviour and other complex phenotypes. *eLife* **10**, e59683 (2021).
 79. W. M. Martin, L. A. Bumm, D. W. McCauley, Development of the viscerocranial skeleton during embryogenesis of the sea lamprey, *Petromyzon marinus*. *Dev. Dyn.* **238**, 3126–3138 (2009).
 80. K. Clement, H. Rees, M. C. Canver, J. M. Gehrke, R. Farouqi, J. Y. Hsu, M. A. Cole, D. R. Liu, J. K. Joung, D. E. Bauer, L. Pinello, CRISPResso2 provides accurate and rapid genome editing sequence analysis. *Nat. Biotechnol.* **37**, 224–226 (2019).
- Acknowledgments:** We thank P. Tafforeau and K. N. Dollman for synchrotron data acquisition and reconstruction. We thank E. E. Wickert and S. M. Miehl (USGS), R. Fraser, D. Mayorga, J. A. Yip, K. C. Lencioni, and A. V. Avalos (Caltech) for help with lamprey husbandry; J. Tan-Cabugao and C. Gonzales for technical assistance; the Caltech Millard and Muriel Jacobs Genetics and Genomics Laboratory and in particular V. Kumar and I. Antoshechkin for preparation and sequencing of RNA-seq libraries; G. Shin from Molecular Technologies for discussion and assistance with probe design; V. Soukup for helpful comments. **Funding:** This work was supported by the National Institutes of Health grant R35NS111564 (M.E.B.), the National Institutes of Health grant F31DE031154 (H.A.U.), the National Institutes of Health grant 1K99/R00HD100587 (M.L.M.), the European Union's Horizon 2020 research and innovation program under Marie Skłodowska-Curie grant agreement no. 897949 (J. Stundl), the Alex's Lemonade Stand Foundation (ALSF) Young Investigator award # 21-24018 (A.R.D.R.), the American Heart Association (AHA) 1020751 (T.S.), the Helen Hay Whitney Foundation (M.L.M.), the Swedish Research Council Vetenskapsrådet 2019-04595 (S.S.), the Swedish Research Council Vetenskapsrådet 2019-04988 (T.H.), and the ESRF-EBS in France LS3021 (S.S., T.H., and J.L.). **Author contributions:** Conceptualization: J. Stundl and M.E.B. Methodology: J. Stundl, A.R.D.R., H.A.U., J.L., T.H., S.S., and M.L.M. Investigation: J. Stundl, A.R.D.R., H.A.U., J.L., J. Stundlo, T.S., T.H., S.S., and M.L.M. Validation: J. Stundl, A.R.D.R., H.A.U., T.H., M.L.M., and M.E.B. Data curation: J. Stundl, A.R.D.R., H.A.U., and J. Stundlo. Formal analysis: J. Stundl, A.R.D.R., J. Stundlo, and Z.M. Visualization: J. Stundl, A.R.D.R., J.L., J. Stundlo, and M.E.B. Resources: J. Stundl, H.A.U., T.H., S.S., M.L.M., and M.E.B. Funding acquisition: J. Stundl, H.A.U., S.S., and M.E.B. Supervision: M.E.B. and T.H. Project administration: J. Stundl and M.E.B. Writing—original draft: J. Stundl and M.E.B. Writing—review and editing: J. Stundl, A.R.D.R., H.A.U., J.L., J. Stundlo, T.S., T.H., S.S., Z.M., M.L.M., and M.E.B. **Competing interests:** The authors declare that they have no competing interests. **Data and materials availability:** All data needed to evaluate the conclusions in the paper are present in the paper and/or the Supplementary Materials. The RNA-seq dataset of the lamprey endostyles generated in this study has been deposited in the National Center for Biotechnology Information Gene Expression Omnibus database (accession no. GSE294220; <https://ncbi.nlm.nih.gov/geo/query/acc.cgi?acc=GSE294220>).
- Submitted 11 December 2024
Accepted 8 July 2025
Published 6 August 2025
10.1126/sciadv.adv2657